Immune Netw. 2023 Jun;23(3):e26
https://doi.org/10.4110/in.2023.23.e26
pISSN 1598-2629·eISSN 2092-6685

IMMUNE NETWORK

Original Article

Check for updates

SARS-CoV-2 Infection Induces HMGB1 Secretion Through Post-Translational Modification and PANoptosis

Man Sup Kwak [1,2,†], **Seoyeon Choi** [1,3,†], **Jiseon Kim** [3,4], **Hoojung Lee** [1,3], **In Ho Park** [2,4], **Jooyeon Oh** [1,3], **Duong Ngoc Mai** [1,5], **Nam-Hyuk Cho** [6,7], **Ki Taek Nam** [3,4], **Jeon-Soo Shin** [1,2,3,*]

[1]Department of Microbiology, Yonsei University College of Medicine, Seoul 03722, Korea
[2]Institute for Immunology and Immunological Diseases, Yonsei University College of Medicine, Seoul 03722, Korea
[3]Brain Korea 21 FOUR Project for Medical Science, Yonsei University College of Medicine, Seoul 03722, Korea
[4]Severance Biomedical Science Institute, Yonsei University College of Medicine, Seoul 03722, Korea
[5]Department of Pediatrics, University of Medicine and Pharmacy, Ho Chi Minh 700000, Vietnam
[6]Department of Microbiology and Immunology, Seoul National University College of Medicine, Seoul 03080, Korea
[7]Department of Biomedical Sciences, Seoul National University College of Medicine, Seoul 03080, Korea

Received: Dec 23, 2022
Revised: Mar 30, 2023
Accepted: Apr 9, 2023
Published online: Apr 24, 2023

***Correspondence to**
Jeon-Soo Shin
Department of Microbiology, Yonsei University College of Medicine, 50-1 Yonsei-ro, Seodaemun-gu, Seoul 03722, Korea.
Email: jsshin6203@yuhs.ac

[†]Man Sup Kwak and Seoyeon Choi contributed equally to this work.

ORCID iDs
Man Sup Kwak
https://orcid.org/0000-0002-3989-3016
Seoyeon Choi
https://orcid.org/0000-0002-3974-2453
Jiseon Kim
https://orcid.org/0000-0002-0979-0278
Hoojung Lee
https://orcid.org/0000-0002-3471-2685
In Ho Park
https://orcid.org/0000-0003-2190-5469
Jooyeon Oh
https://orcid.org/0000-0003-1701-7792

ABSTRACT

Severe acute respiratory syndrome coronavirus 2 (SARS-CoV-2) infection induces excessive pro-inflammatory cytokine release and cell death, leading to organ damage and mortality. High-mobility group box 1 (HMGB1) is one of the damage-associated molecular patterns that can be secreted by pro-inflammatory stimuli, including viral infections, and its excessive secretion levels are related to a variety of inflammatory diseases. Here, the aim of the study was to show that SARS-CoV-2 infection induced HMGB1 secretion via active and passive release. Active HMGB1 secretion was mediated by post-translational modifications, such as acetylation, phosphorylation, and oxidation in HEK293E/ACE2-C-GFP and Calu-3 cells during SARS-CoV-2 infection. Passive release of HMGB1 has been linked to various types of cell death; however, we demonstrated for the first time that PANoptosis, which integrates other cell death pathways, including pyroptosis, apoptosis, and necroptosis, is related to passive HMGB1 release during SARS-CoV-2 infection. In addition, cytoplasmic translocation and extracellular secretion or release of HMGB1 were confirmed via immunohistochemistry and immunofluorescence in the lung tissues of humans and angiotensin-converting enzyme 2-overexpressing mice infected with SARS-CoV-2.

Keywords: HMGB1 protein; Severe acute respiratory syndrome coronavirus 2; Post-translational modification; PANoptosis

INTRODUCTION

Coronaviruses (*Coronaviridae*) are positive-sense single-stranded RNA viruses that cause diseases in mammals and birds, and were first discovered in the 1960s (1). Severe acute respiratory syndrome coronavirus 2 (SARS-CoV-2), recently identified in Wuhan, China in December 2019, was declared a pandemic by the World Health Organization in March 2020.

Duong Ngoc Mai
https://orcid.org/0000-0002-6217-604X
Nam-Hyuk Cho
https://orcid.org/0000-0003-3673-6397
Ki Taek Nam
https://orcid.org/0000-0001-5292-1280
Jeon-Soo Shin
https://orcid.org/0000-0002-8294-3234

Conflict of Interest
The authors declare no potential conflicts of interest.

Abbreviations
ACE2, angiotensin-converting enzyme 2; COVID-19, coronavirus disease 2019; DAMP, damage-associated molecular pattern; dpi, days post-infection; GSDMD, Gasdermin-D; HMGB1, high-mobility group box 1; hpi, hours post-infection; IAV, influenza A virus; MLKL, mixed lineage kinase domain-like protein; MOI, multiplicity of infection; NP, nucleocapsid protein; p-, phospho-; PANoptosis, pyroptosis, apoptosis, and necroptosis; PFU, plaque-forming unit; PTM, post-translational modification; RdRp, RNA-dependent RNA polymerase; RIPK3, receptor interacting serine/threonine kinase 3; RT, room temperature; SARS-CoV-2, severe acute respiratory syndrome coronavirus 2; TBS, Tris-buffered saline; TMPRSS2, transmembrane protease serine S1 member 2; WCL, whole-cell lysate; ZBP1, Z-DNA binding protein 1.

Author Contributions
Data curation: Choi S; Formal analysis: Choi S; Funding acquisition: Shin JS, Kwak MS; Investigation: Choi S, Kim J, Lee H, Park IH, Oh J; Methodology: Lee H, Park IH, Oh J, Nam KT; Project administration: Shin JS; Resources: Cho NH, Nam KT; Supervision: Shin JS, Kwak MS; Validation: Mai DN; Visualization: Choi S, Kim J; Writing - original draft: Kwak MS, Choi S; Writing - review & editing: Shin JS.

It has continuously mutated and evolved into many variants by modifying the spike protein sequence and structure (2-4). SARS-CoV-2 surface spike proteins bind to angiotensin-converting enzyme 2 (ACE2) on the surface of lung, lymph, and respiratory epithelial cells, and, eventually, SARS-CoV-2 enters host cells through the cell surface entry pathway or endocytosis (5-7). SARS-CoV-2 spike protein and ACE2 cellular attachment are essential for cell surface entry, and subsequent entry mechanisms depend on proteases of transmembrane protease serine S1 member 2 (TMPRSS2) (8). However, when host cells do not express sufficient TMPRSS2 on the cell surface, or when SARS-CoV-2 and ACE2 complexes do not encounter TMPRSS2, SARS-CoV-2 is internalized via clathrin-mediated endocytosis (9). After SARS-CoV-2 invades and replicates inside the host cells, the innate immune system is activated as an early defense mechanism for viral infection (10). This induces various types of inflammatory cell death, and the cell releases damage-associated molecular patterns (DAMPs) to alarm the surrounding environment regarding homeostatic imbalance (11-14).

In particular, SARS-CoV-2 triggers multiple simultaneous inflammatory cell death that is called PANoptosis. PANoptosis, which has been recently identified, is a Z-DNA binding protein 1 (ZBP1)-dependent inflammatory cell death pathway. ZBP1 recognition of the influenza A virus (IAV) proteins, such as nucleocapsid protein (NP) and RNA polymerase subunit PB1, induces NLRP3 inflammasome activation and PANoptosis in IAV-infected cells. ZBP1-deficient mice are protected against inflammatory responses and epithelial damage during IAV infection (15). In addition, the innate immune sensor AIM2 forms a complex with pyrin and ZBP1 and induces PANoptosis (16). PANoptosis includes pyroptosis, necroptosis, and apoptosis-associated factors, but considering its unique inflammasome complex, the PANoptosome, these factors alone cannot explain PANoptosis. According to recent studies, PANoptosis can lead to a cytokine storm during SARS-CoV-2 infection (17). The severity of SARS-CoV-2 in patients is associated with a cytokine storm due to elevated levels of circulating chemokines and cytokines, including TNF-α, IFN-γ, IL-6, IL-8, IL-1α, and IL-1β (13,18). Cytokine storms are associated with hyperactivation of the immune system and excessive cytokine release, ultimately causing multi-organ damage. Partial or mixed blockade of cytokines such as TNF-α and IFN-γ has been successful in treating cytokine storm associated diseases (13). In fact, IFN-β induces ZBP1-mediated PANoptosis. IFN-β treatment increased lethality in coronavirus-infected mice, but genetic deletion of *Zbp1* mice was protective (17). Secretion levels of high-mobility group box1 (HMGB1), a late mediator of lethal systemic inflammation (19), are increased in blood along with those of other cytokines with severe SARS-CoV-2 infection (20).

HMGB1 is one of the DAMPs associated with many inflammatory diseases and infections. HMGB1 is a highly abundant and ubiquitously expressed protein that functions as a DNA chaperone, once actively secreted or passively released (21-27). Post-translational modifications (PTMs) of HMGB1 such as acetylation, phosphorylation, *N*-glycosylation, methylation, oxidation, and ADP-ribosylation play important roles in both nuclear-cytoplasmic transport and extracellular secretion (28-33). HMGB1 contains 3 cysteine residues, and their redox state determines its role as a DAMP. Reduced HMGB1 (all cysteine residues in the thiol state) exhibits chemotactic functions (34), and oxidized HMGB1 (intramolecular disulfide bond between Cys23 and Cys45) exhibits pro-inflammatory functions (35). Sulfonic HMGB1 (all 3 cysteine residues in the hyperoxidized sulfonic acid state) does not exhibit chemotactic or pro-inflammatory functions (36). The formation of intramolecular disulfide bonds between Cys23 and Cys45 in HMGB1 is facilitated by peroxiredoxin I/II under inflammatory stimulation (32). Furthermore, HMGB1 is passively

released by diverse cell death, such as pyroptosis, necroptosis, apoptosis, and necrosis (37-39). Extracellular HMGB1 binds to various receptors such as the receptor for advanced glycation end products and TLR-2, -4, and -9, which then activate the downstream signaling pathway to enhance the inflammatory and immune responses (23,40-43). Excessive extracellular HMGB1 is responsible for a variety of immune pathogeneses (44-46).

In the present study, we observed a physiological relationship between SARS-CoV-2 infection and HMGB1 secretion. HMGB1 extracellular secretion depended on the time after SARS-CoV-2 infection. Nuclear-to-cytoplasmic and cytoplasmic-to-extracellular translocation of HMGB1 included both active secretion via PTMs and passive release via PANoptosis. Thus, inhibition of HMGB1 secretion may ameliorate cytokine storms and septic shock caused by SARS-CoV-2.

MATERIALS AND METHODS

Cell cultures and transfection

HEK293E/ACE2-C-GFP (human embryonic kidney cells), a human ACE2 overexpressed-HEK293E stable cell line, was a gift from Y-Biologics Inc. (W0064; Daejeon, Korea). The Calu-3 (human lung epithelial) cell line was obtained from the Korea Cell Line Bank (Seoul, Korea). HEK293E/ACE2-C-GFP cells were cultured in DMEM supplemented with 10% FBS, 100 U/ml penicillin, and 100 μg/ml streptomycin and incubated at 37°C under 5% CO_2. HEK293E/ACE2-C-GFP cells were selected using 200 μg/ml hygromycin B (Invitrogen, Carlsbad, CA, USA). Calu-3 cells were cultured in Eagle's minimum essential medium supplemented with 10% FBS, 100 U/ml penicillin, and 100 μg/ml streptomycin, and incubated at 37°C under 5% CO_2. Cells were plated for 24 h and grown to 80%–90% confluency for plasmid transfection. Transfection was carried out using the Fugene HD reagent (Promega Corporation, Madison, WI, USA) for HEK293E/ACE2-C-GFP cells and an electroporation system (Invitrogen) by MicroPorator-mini (Digital Bio, New York, NY, USA) for Calu-3 cells.

Virus production and titration

SARS-CoV-2 (BetaCoV/Korea/KCDC03/2020, NCCP 43326) was obtained from the National Culture Collection for Pathogens, Korea Disease Control and Preventive Agency (Osong, Korea). The SARS-CoV-2 virus was amplified in Vero cells (American Type Culture Collection, Manassas, VA, USA) until the cell cytopathic effect was observed in over 80% of the cells (48–72 h). The supernatants were centrifuged at 20,000 × g, passed through a 0.45-μm filter, aliquoted, and stored at −80°C. The virus stock was titrated using a plaque assay. Typical titers were 1×10^7 plaque-forming units (PFU)/ml.

HEK293E/ACE2-C-GFP and Calu-3 cells were grown on poly-L-lysine coated plates overnight at 37°C and infected with SARS-CoV-2 for the indicated time at a multiplicity of infection (MOI) of 0.1 or 1 for each experiment. Cells and culture supernatants were harvested, and total RNA was extracted manually using the easy-Blue™ total RNA extraction kit (iNtRON Biotechnology, Seongnam, Korea). SARS-CoV-2 infectivity was analyzed via real-time PCR using QuantStudio 3 (Thermo Fisher Scientific, Waltham, MA, USA). SARS-CoV-2 RNA-dependent RNA polymerase (RdRp) primers and probes were used for the one-step real-time PCR. The sequences of the RdRp primers used were 5′-GTGARATGGTCATGTGTGGCGG-3′ and 5′-CARATGTTAAASACACTATTAGCATA-3′. The probe sequence was

https://doi.org/10.4110/in.2023.23.e26

5′-CAGGTGGAACCTCATCAGGAGATGC-3′ (Macrogen, Seoul, Korea). An in-house standard curve based on PFU was established using the RdRp mRNA copy number, and each infected sample was quantified based on the standard curve.

Western blot analysis and immunoprecipitation

HEK293E/ACE2-C-GFP and Calu-3 cells were seeded on poly-L-lysine-coated 6-well plates and infected with SARS-CoV-2 at an MOI of 0.1 for 6, 24, and 48 h. Cells were washed with PBS and lysed in 1× RIPA buffer (GenDEPOT, Katy, TX, USA) containing 150 mM NaCl, 1% Triton X-100, 1% deoxycholic acid sodium salt, 0.1% SDS, 50 mM Tris-HCl pH 7.5, and 2 mM EDTA and a protease inhibitor cocktail (GenDEPOT) and phosphatase inhibitor cocktail (GenDEPOT). Cells in 1× RIPA buffer were gently rocked for 1 h at 4°C. Whole-cell lysates (WCLs) were centrifuged at 20,000 × g for 15 min at 4°C. Reducing protein sample buffer (100 mM Tris-HCl pH 6.8, 2% SDS, 25% glycerol, 0.1% bromophenol blue, and 5% β-mercaptoethanol) and non-reducing protein sample buffer (100 mM Tris-HCl pH 6.8, 2% SDS, 25% glycerol, 0.1% bromophenol blue) were added to equal WCL protein aliquots. The WCL with reducing protein sample buffer are followed by heating at 95°C for 10 min. Proteins were separated via SDS-PAGE or non-reducing SDS-PAGE and then transferred to nitrocellulose membranes (GE Healthcare, Chicago, IL, USA). Nonspecific binding sites were blocked with Tris-buffered saline (TBS) containing 0.1% Tween 20 and 5% (w/v) skim milk for 1 h. After blocking, membranes were incubated with anti-SARS-CoV/SARS-CoV-2 NP (Sinobiological, Beijing, China), anti-HMGB1 (Abcam, Cambridge, UK), anti-β-actin (Cell Signaling Technology, Danvers, MA, USA), anti-gasdermin-D (GSDMD; Abcam), anti-phospho mixed lineage kinase domain-like protein (p-MLKL; Cell Signaling Technology), anti-MLKL (Novus Biologicals, Englewood, CO, USA), anti-cleaved-caspase-3 (Cell Signaling Technology), anti-pRIPK3 (Abcam), and anti-cleaved-caspase-8 (Cell Signaling Technology) Abs at 4°C overnight. Membranes were washed 3 times with TBS containing 0.1% Tween 20 and incubated with the appropriate HRP-conjugated secondary Abs (Jackson ImmunoResearch, West Grove, PA, USA) at room temperature (RT) for 1 h. After washing 3 times, an enhanced chemiluminescence substrate with 3,3',5,5'-tetramethylbenzidine solution (GenDEPOT) was used for visualization.

Immunoprecipitation was performed with 200 μg of WCL protein. Initially, 1 μg of anti-HMGB1 Ab (R&D systems, Minneapolis, MN, USA) was conjugated with Dynabeads® Protein G (Bio-Rad, Hercules, CA, USA) at RT for 1 h. WCLs were added to anti-HMGB1 Ab-conjugated Dynabeads® Protein G and incubated at 4°C for 18 h. The beads were washed 3 times with PBS containing 0.01% Tween 20, mixed with protein sample buffer, and heated at 95°C for 10 min. The proteins were separated using SDS-PAGE and immunoblotted with anti-phospho-serine/threonine (Abcam), anti-acetyl-lysine (Abcam), and anti-HMGB1 (Abcam) Abs.

Measurement of HMGB1 secretion

To analyze HMGB1 secretion in the supernatants, culture media were replaced with serum-free Opti-minimum essential medium (Gibco®, Grand Island, NY, USA). Cells were pre-treated with or without 1 μM or 5 μM GSK-872 for 24 h, and 10 μM or 50 μM Z-IETD-fmk for 1 h. Cells with inhibitors were infected with SARS-CoV-2 at an 0.1 MOI for 48 h, and cells without inhibitors were infected with SARS-CoV-2 at 0.1 MOI for 6, 24, and 48 h. The culture supernatants were harvested and concentrated via methanol precipitation after removing the cell debris. Ice-cold methanol and chloroform were added to the culture supernatants, and the mixture was centrifuged at 2,000 × g for 10 min. The upper area above the protein layer was quickly removed, methanol was added at a ratio of a quarter of the supernatant, and then

centrifuged at 20,000 × g for 10 min at 4°C. Supernatants were removed, and protein sample buffer was added to the protein pellet, followed by heating at 95°C for 10 min. Western blot analysis was performed using anti-HMGB1 Ab (Abcam).

Immunohistochemistry and immunofluorescence

Lung tissue was fixed with 4% paraformaldehyde, embedded in paraffin wax, and sectioned at a thickness of 4 μm. After deparaffinization and rehydration, the sections were retrieved in citrate buffer (pH 6.0; Agilent Technologies DAKO, Santa Clara, CA, USA) under high-pressure cooking, cooled on ice, and incubated in 3% H_2O_2 to inactivate endogenous peroxidase. After washing twice with PBS, the sections were blocked with blocking buffer (Agilent Technologies DAKO) at RT. The sections were incubated with anti-HMGB1 (Abcam), anti-SARS-CoV/SARS-CoV-2 NP (Sinobiological), anti-F4/80 (Cell Signaling Technology), anti-CD3ε (Cell Signaling Technology), anti-CD45R (Abcam), and anti-neutrophil [NIMP-R14] (Abcam) Abs overnight at 4°C. The sections were then incubated with a secondary Ab conjugated with HRP (Agilent Technologies DAKO) for 15 min. 3,3'-diaminobenzidine substrate (Agilent Technologies DAKO) was used to develop the immunohistochemical signal, and Mayer's hematoxylin was used to stain the nucleus. For immunofluorescence, after primary Ab treatment, the sections were incubated with anti-rabbit conjugated with Cy3 (Abcam) or anti-mouse Alexa Fluor 488 (Invitrogen) for 1 h at RT. The sections were mounted with a mounting solution containing DAPI (Vector Laboratories, Burlingame, CA, USA). Immunofluorescence imaging was performed using EVOS-FL imaging systems (Thermo Fisher Scientific) and LSM-980 confocal microscope (Carl Zeiss, Oberkochen, Germany).

Confocal microscopy

HEK293E/ACE2-C-GFP cells were grown in a poly-L-lysine-coated LabTekTM II chamber (Thermo Fisher Scientific) for 24 h and transfected with HMGB1-mCherry plasmid for 24 h. Calu-3 cells were transfected with HMGB1-mCherry plasmid using an electroporation system by following the company manual. Calu-3 cells were then seeded in a poly L-lysine-coated chamber for 24 h. Cells were infected with SARS-CoV-2 at 1 MOI for 6, 24, and 48 h. Cells were fixed with 4% paraformaldehyde in PHEM buffer for 20 min at RT and then washed 3 times with cold PBS. After mounting with DAPI, HMGB1-mCherry, ACE2-GFP, propidium iodide, and DAPI were observed using an FV1000 (Olympus, Tokyo, Japan) or LSM-700 (Carl Zeiss) confocal microscope.

Mouse and human autopsy study

Seven- to 8-week-old male K18-hACE2 mice [B6.Cg-Tg(K18-ACE2)2PrImn/J] were purchased from the Jackson Laboratory (Bar Harbor, ME, USA). All experiments were performed in accordance with the Public Health Service and Humane Care and Use of Laboratory Animal Care-accredited unit, and the protocols were approved by the Institutional Animal Care and Use Committee of Yonsei Laboratory Animal Research Center (YLARC, 2020-0216). All experiments were conducted in an Animal Biosafety Level 3 facility at Yonsei University College of Medicine under safety guidelines and control. K18-hACE2 mice were anesthetized with a Zoletil–Rompun mixture (4:1) and then administered 50 μl of SARS-CoV-2 virus (1×10^4 PFU) via the intranasal route. At 7 days post-infection (dpi), mouse lung samples were collected for immunohistochemistry or immunofluorescence, and mouse serum samples were collected to measure secreted HMGB1.

Paraffin-embedded human lung autopsy sections from coronavirus disease 2019 (COVID-19) patients were prepared from the author's previous report, in which all the information for study participants and ethics statement are described in detail (47).

Statistical analysis

Band density was calculated with the image analysis program using ImageJ software (Version 1.53; National Institutes of Health, Bethesda, MD, USA), and experimental data were analyzed via either Student's *t*-test or one-way ANOVA using GraphPad Prism (version 9.0.0; GraphPad Software, San Diego, CA, USA). A p-value <0.05 was considered statistically significant.

RESULTS

SARS-CoV-2 infection induces HMGB1 release

SARS-CoV-2 entry into host cells depends on ACE2, which leads to inflammatory responses and cell death (5). First, we assessed SARS-CoV-2 infectivity over time in HEK293E/ACE2-C-GFP and Calu-3 cells. We consistently observed that SARS-CoV-2 replicated rapidly around 24 h post-infection (hpi) and showed an explosively growing RdRp copy number until 48 hpi in both intracellular and extracellular environments (**Fig. 1A-D**). Similarly, SARS-CoV-2 NP

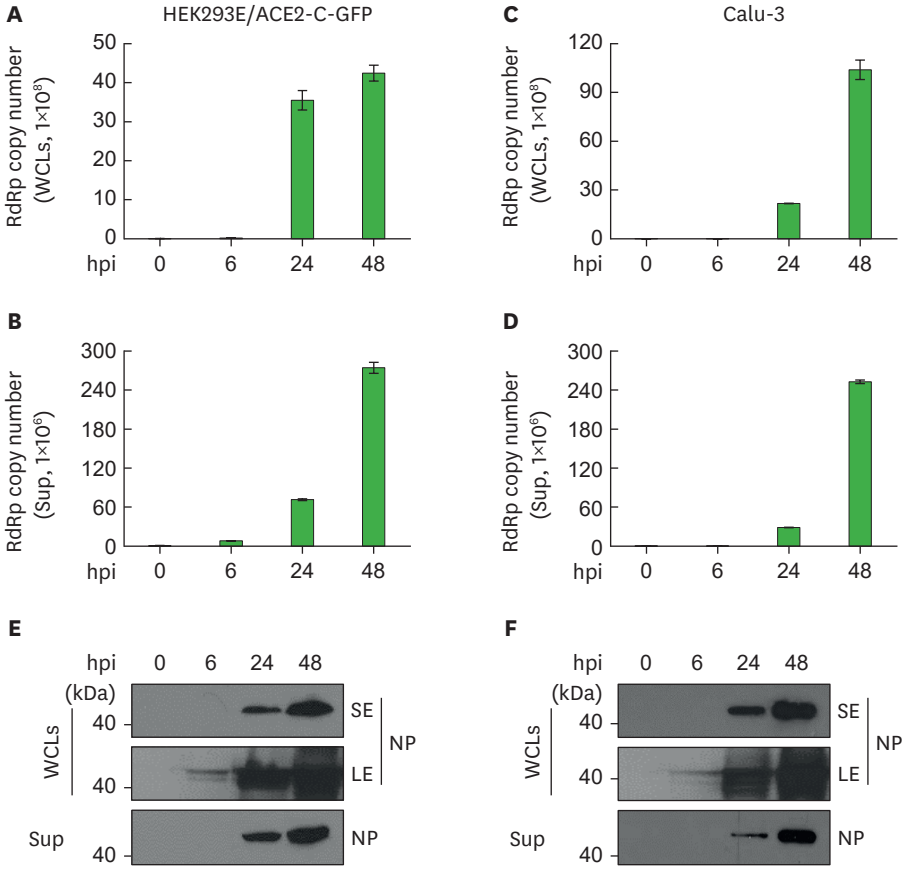

Figure 1. SARS-CoV-2 replication in HEK293E/ACE2-C-GFP and Calu-3 cells. HEK293E/ACE2-C-GFP and Calu-3 cells were infected with 0.1 MOI SARS-CoV-2 for 6, 24, and 48 h, and then WCLs and Sup were collected for quantitative real-time PCR and western blotting. WCLs (A, C) and culture supernatants (B, D) of HEK293E/ACE2-C-GFP and Calu-3 cells were subjected to quantitative real-time PCR (A-D) and immunoblotted with anti-SARS-CoV-2 NP Ab (E, F). Sup, supernatant; SE, short exposure; LE, long exposure.

https://doi.org/10.4110/in.2023.23.e26

was mainly detected around 24 hpi, and was strongly enhanced at 48 hpi in both WCLs and supernatants of both cell lines in Western blot analysis (**Fig. 1E and F**).

According to a previous report, HMGB1 is released after Newcastle disease virus infection and decreases viral replication by increasing inflammation (48,49). Thus, we investigated the physiological relevance of HMGB1 translocation and SARS-CoV-2 infection. To examine the cytoplasmic translocation and extracellular secretion of HMGB1 in response to SARS-CoV-2 infection, HEK293E/ACE2-C-GFP and Calu-3 cells were transfected with mCherry-tagged HMGB1 plasmids. With respect to our results, 6, 24, and 48 hpi were considered appropriate time points to observe the correlation between HMGB1 translocation and SARS-CoV-2 infection (**Fig. 2A-D**).

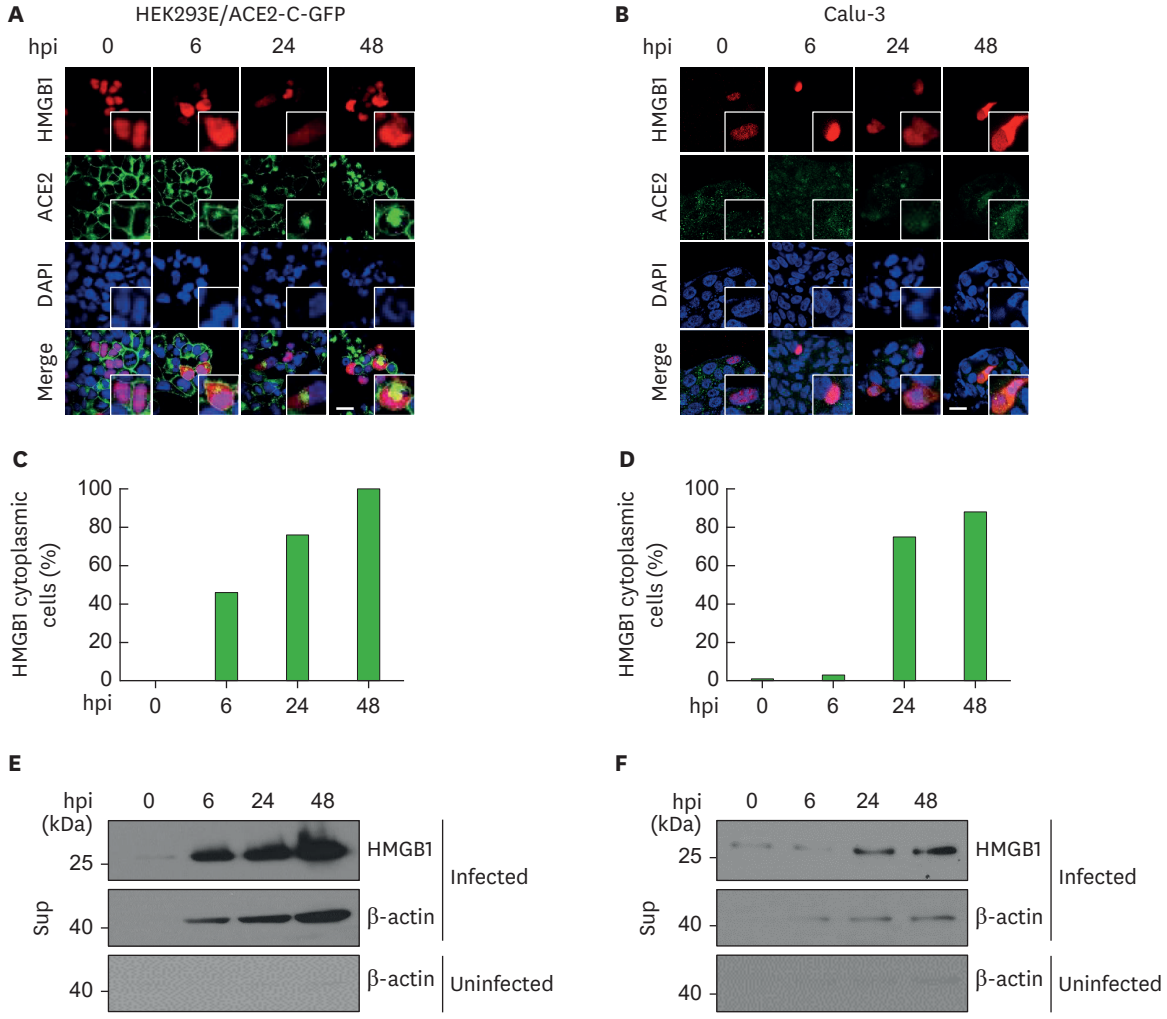

Figure 2. SARS-CoV-2 infection-induced HMGB1 release. HEK293E/ACE2-C-GFP (A) and Calu-3 cells (B), which were transiently transfected with mCherry-tagged HMGB1, were infected with 1 MOI SARS-CoV-2 for 6, 24, and 48 h and examined for mCherry fluorescence via confocal microscopy. An enlarged image is in the box (scale bar=20 μm). (C, D) The number of cytoplasmic mCherry-HMGB1-positive cells was determined using the ImageJ program (n>100). HEK293E/ACE2-C-GFP (E) and Calu-3 (F) cells were infected with 0.1 MOI SARS-CoV-2 for 6, 24, and 48 h. Culture Sup were harvested, and subjected to western blot analysis using anti-HMGB1 and anti-β-actin Abs.
Sup, supernatant.

https://doi.org/10.4110/in.2023.23.e26

HMGB1 underwent cytoplasmic translocation in the early stages of SARS-CoV-2 infection in HEK293E/ACE2-C-GFP cells (**Fig. 2A and C**). The cytoplasmic translocation of HMGB1 was slightly delayed in Calu-3 cells (**Fig. 2B and D**), probably because of the difference in ACE2 receptor expression (**Supplementary Fig. 1**). Immunoblotting analysis of culture supernatants revealed that SARS-CoV-2 infection induced the extracellular secretion of endogenous HMGB1 in both cell lines (**Fig. 2E and F**). Extracellular HMGB1 was first detected at 6 hpi in HEK293E/ACE2-C-GFP cells and at 24 hpi in Calu-3 cells. This corresponds to the cytoplasmic translocation of HMGB1, as shown via confocal image analysis. β-actin was also immunoblotted in the culture supernatants of infected cells, similar to the pattern of HMGB1 release in both cell types (**Fig. 2E and F**). These results suggested that HMGB1 secretion is associated with SARS-CoV-2-related inflammation and cell death.

SARS-CoV-2 induces PTMs of HMGB1

The extracellular secretion of HMGB1 is related to 2 separate mechanisms: active secretion and passive release (27,50). PTMs of HMGB1, such as acetylation, phosphorylation, and oxidation, are involved in the active secretion mechanism. To confirm the active secretion of HMGB1 by SARS-CoV-2 infection, we investigated PTMs of HMGB1 during SARS-CoV-2 infection. Oxidized HMGB1 was observed in WCLs of both HEK293E/ACE2-C-GFP and Calu-3 under non-reducing SDS-PAGE in a time-dependent manner after SARS-CoV-2 infection. The dimeric form of HMGB1, present under oxidative stress (51), was observed after 6 hpi in both cell lines (**Fig. 3A and B**). HMGB1 acetylation and phosphorylation after SARS-CoV-2 infection were analyzed using immunoprecipitation and observed after 6 hpi in HEK293E/ACE2-C-GFP and Calu-3 cells (**Fig. 3C and D**). These results show that SARS-CoV-2 infection influences PTMs of HMGB1, leading to its secretion.

SARS-CoV-2 induces HMGB1 release through PANoptosis

HMGB1 can be passively released during various forms of cell death, such as pyroptosis, necroptosis, apoptosis, and necrosis (27,50). To investigate the link between SARS-CoV-2-

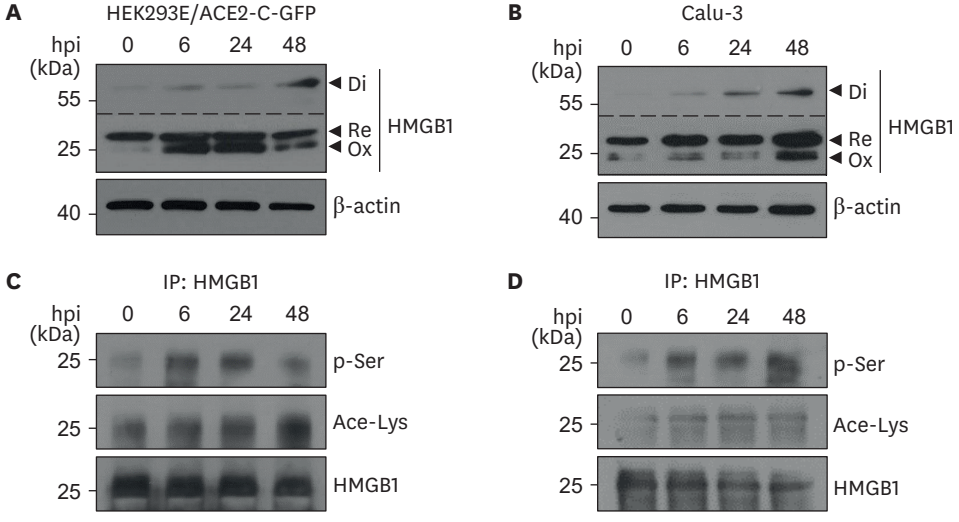

Figure 3. SARS-CoV-2 infection-induced post-translational modifications of HMGB1. HEK293E/ACE2-C-GFP (A) and Calu-3 (B) cells were infected with 0.1 MOI SARS-CoV-2 for 6, 24, and 48 h, after which WCLs were subjected to non-reducing SDS-PAGE and immunoblotting. HEK293E/ACE2-C-GFP (C) and Calu-3 (D) cells were infected with 0.1 MOI SARS-CoV-2, and WCLs were immunoprecipitated with anti-HMGB1 Abs, immunoblotted with anti-p-Ser and anti-Ace-Lys Abs, and reblotted with anti-HMGB1 Abs.
Re, reduced HMGB1; Ox, oxidized HMGB1; Di, dimerized HMGB1; p-Ser, phospho-serine; Ace-Lys, acetyl-lysine.

https://doi.org/10.4110/in.2023.23.e26

infected cell death and HMGB1 release, PANoptosis was observed during viral infection. First, we determined whether SARS-CoV-2 infection induces pyroptosis. Gasdermin-D (GSDMD)-N terminal band, an activated form of GSDMD, was clearly observed at 24 and 48 hpi in both cell lines (**Fig. 4A and B**). In addition, viral infection in HEK293E/ACE2-C-GFP and Calu-3 cells occurred through cleavage of the apoptosis activator caspase-3 (**Fig. 4A and B**). Next, we investigated whether SARS-CoV-2 infection causes necroptosis. Infection induced phosphorylation of the necroptosis marker p-MLKL, which stimulated serial necroptotic events, in a time-dependent manner (**Fig. 4A and B**). Remarkably, MLKL and p-MLKL were observed around 35 kDa in HEK293E/ACE2-C-GFP cells, which is not the generally expected size (up to 54 kDa) in other cell lines. Likewise, previous report showed that p-MLKL was also detected at 35 kDa in human multiple myeloma and RPMI8226 cell lines (52), and 35 kDa of MLKL was observed in HEK293E/ACE2-C-GFP cells. We also confirmed an increase in the propidium iodide fluorescence signal in HEK293E/ACE2-C-GFP and Calu-3 cells 48 hpi (**Fig. 4C and D**). It has previously been shown that activation of PANoptosis is dependent on phospho-receptor interacting serine/threonine kinase 3 (RIPK3)/caspase-8 independent of the trigger (16). To determine whether HMGB1 secretion could be regulated by inactivation of RIPK3 and caspase-8, we used GSK872, a selective RIPK3 inhibitor that binds RIPK3 domain, and Z-IETD-fmk, a specific caspase-8 inhibitor. We confirmed that HMGB1 secretion was significantly reduced by the inhibitors in a dose-dependent manner in both cell types (**Fig. 4E and F**). Double knock-down of RIPK3 and caspase-8 also reduced HMGB1 secretion (**Supplementary Fig. 2**). However, recombinant HMGB1 alone has no effect on PANoptosis (**Supplementary Fig. 3**). These results suggest that HMGB1 secretion after SARS-CoV-2 infection is associated with PANoptosis.

HMGB1 release in mice and human lung tissues after SARS-CoV-2 infection

Human ACE2-expressing K18-hACE2 mice were infected intranasally with a sublethal dose (1×10^4 PFU) of SARS-CoV-2. Blood was collected at 0 and 7 dpi to detect HMGB1 in serum samples from 2 mice for each time point, and HMGB1 levels were analyzed using non-reducing SDS-PAGE. Its levels significantly increased after SARS-CoV-2 infection, and HMGB1, including dimeric HMGB1, was detected at 7 dpi (**Fig. 5A**). Immunohistochemistry and immunofluorescence assays were performed to identify cytoplasmic HMGB1 during SARS-CoV-2 infection. SARS-CoV-2 NP was highly expressed in the alveoli and interstitial locations of the mouse lungs at 7 dpi. In addition, the lung tissue was infiltrated by numerous immune cells and showed damaged alveolar structures, including alveolar wall thickening (**Fig. 5B**). Cytoplasmic HMGB1-positive cells significantly increased, compared with those in uninfected lungs (**Fig. 5C**). Similar results were obtained in the immunofluorescence assay. The number of cytoplasmic HMGB1-positive cells at 7 dpi in SARS-CoV-2-infected lungs increased 11.32-fold, compared with that in uninfected lungs (**Fig. 5D and E**). To determine which types of immune cell infiltrated in the damaged lungs of 7 dpi mice, we performed the immunohistochemistry to detect 4 types of immune cells with appropriate markers. F4/80 was used to detect macrophages, CD3ε was used for T cells, CD45R was used for B cells, and anti-neutrophil (NIMP-R14) Ab for neutrophils. We confirmed that all types of immune cells were dramatically increased at 7 dpi compared to uninfected mice (**Fig. 5F-H**). We performed an immunofluorescence assay using lung tissues from a healthy individual and postmortem autopsy samples of patients with SARS-CoV-2. The expression of SARS-CoV-2 NP was observed in autopsied lungs (**Fig. 6A**). The number of cytoplasmic HMGB1-positive cells in the 2 autopsy lung samples increased by 2.98-fold and 3.18-fold, compared with that in normal lungs (**Fig. 6B and C**). These results demonstrated that HMGB1 release is strongly associated with the disease severity of SARS-CoV-2 infection in both murine and humans.

https://doi.org/10.4110/in.2023.23.e26

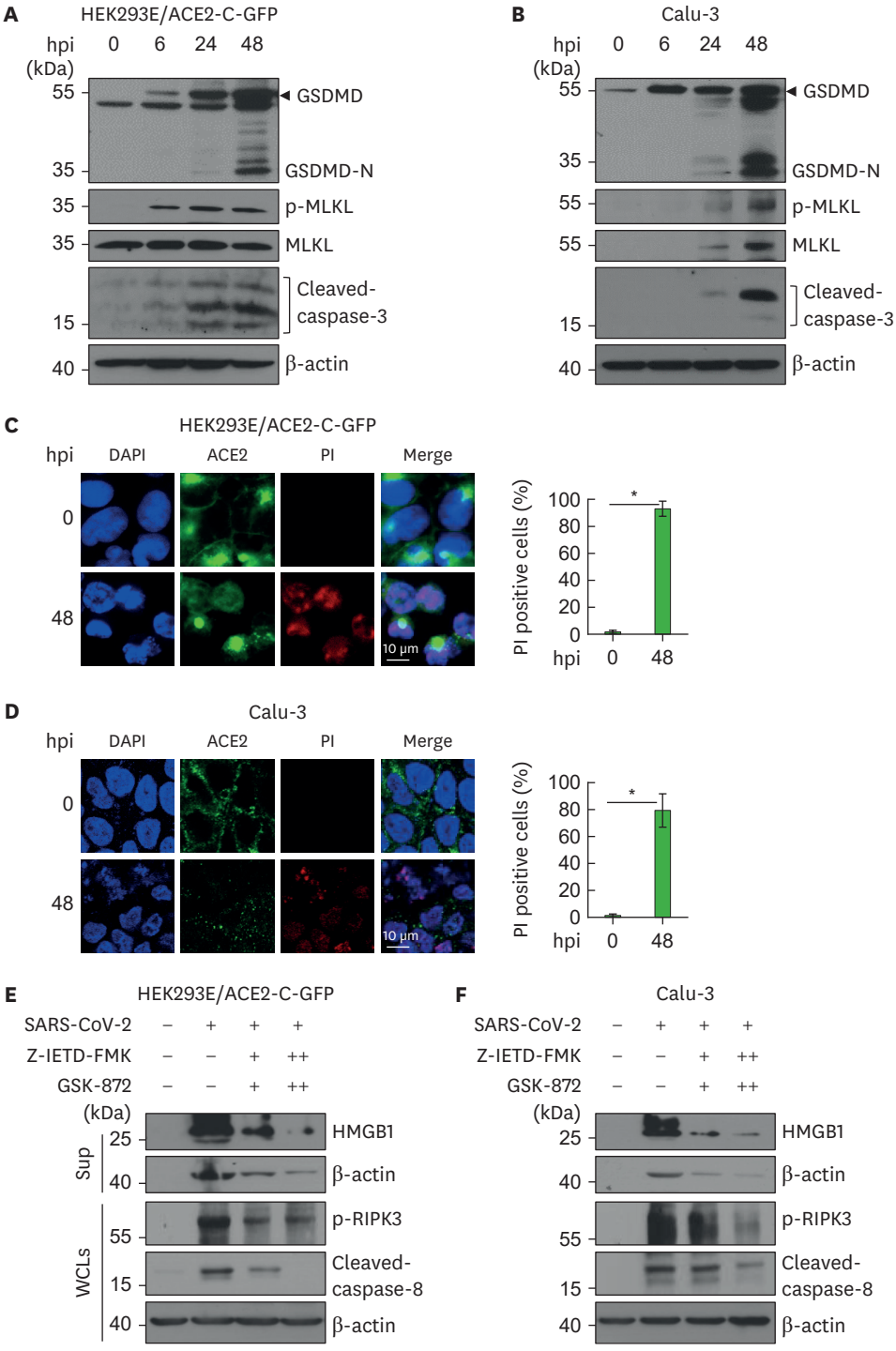

Figure 4. SARS-CoV-2 infection induced HMGB1 release through PANoptosis. HEK293E/ACE2-C-GFP (A) and Calu-3 (B) cells were infected with 0.1 MOI SARS-CoV-2 for 6, 24, and 48 h, after which WCLs were subjected to SDS-PAGE and immunoblotted with anti-GSDMD, anti-p-MLKL, anti-MLKL, anti-cleaved-caspase-3, and anti-β-actin Abs. HEK293E/ACE2-C-GFP (C) and Calu-3 (D) cells were infected with 1 MOI SARS-CoV-2 for 48 h, and dead cells were stained with propidium iodide. The percentage of propidium iodide-positive cells (red) were determined. Data are presented as means ± SD (n=4). (E, F) HEK293E/ACE2-C-GFP and Calu-3 cells were pre-treated with 1 μM (+) and 5 μM (++) GSK-872 for 24 h, and 10 μM (+) and 50 μM (++) Z-IETD-fmk for 1 h, followed by infection with 0.1 MOI SARS-CoV-2 for 48 h. WCLs were subjected to SDS-PAGE and immunoblotted to observe p-RIPK3, cleaved-caspase-8 and β-actin. Culture Sup were harvested, and subjected to Western blot analysis using anti-HMGB1 and anti-β-actin Abs.
Sup, supernatant.
*p<0.001 vs. 0 hpi, *t*-test.

https://doi.org/10.4110/in.2023.23.e26

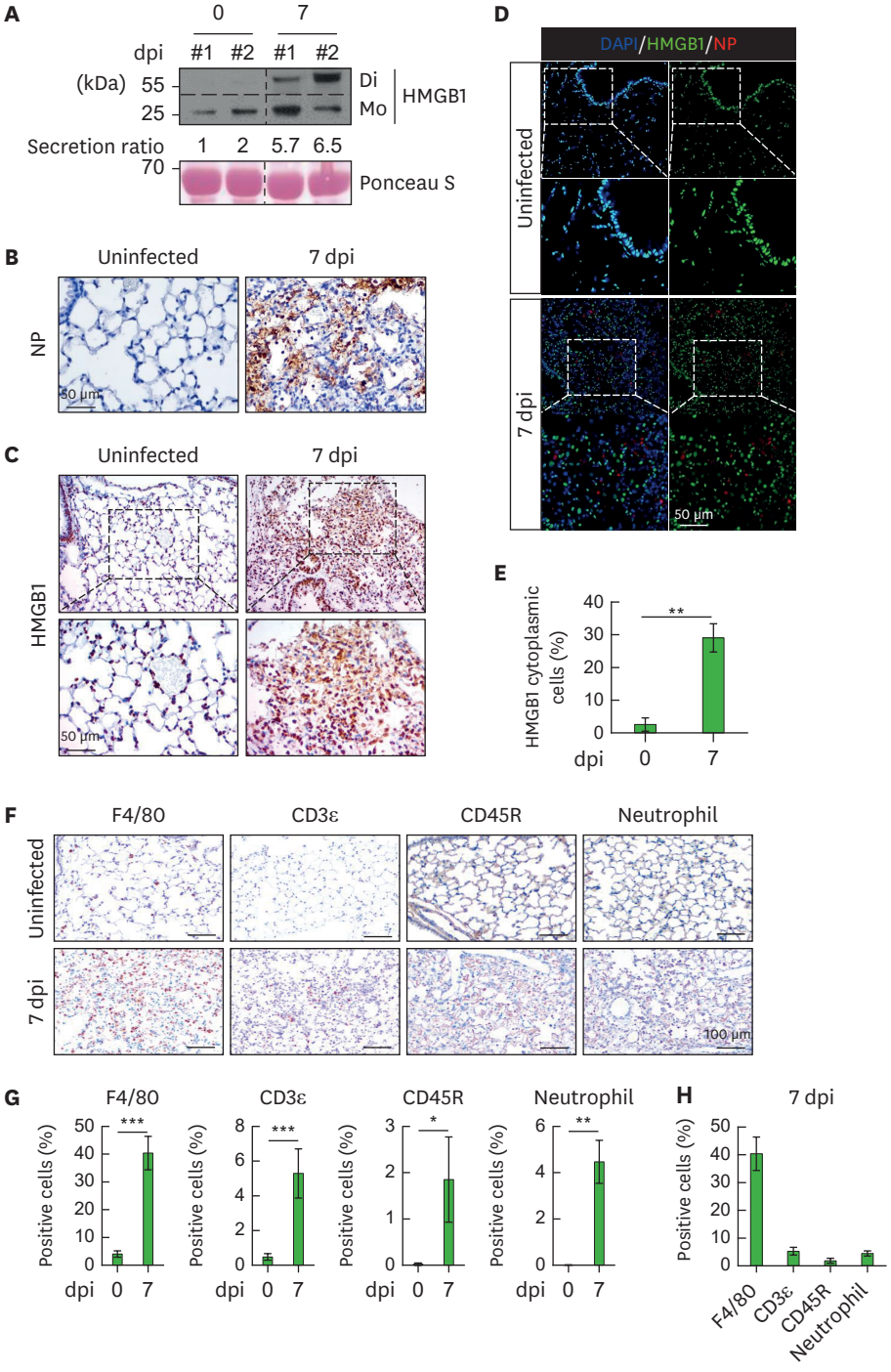

Figure 5. SARS-CoV-2 infection-induced cytoplasmic translocation of HMGB1 in mice. (A-D) K18-hACE2 mice (n=2) received SARS-CoV-2 (1×10^4 PFU) intranasally for 7 days. Mice were euthanized to collect serum to determine extracellular HMGB secretion level in lung tissues to confirm the cytoplasmic localization of HMGB1. (A) HMGB1 serum levels were subjected to non-reducing SDS-PAGE and immunoblotted with anti-HMGB1 Abs. Ponceau-S staining of Rubisco was used as a loading control. (B, C) Lung sections from uninfected (n=2) or SARS-CoV-2-infected (n=2) mice were subjected to immunohistochemistry using anti-SARS-CoV-2 NP (B) and anti-HMGB1 (C) Abs. (D) Immunostaining of HMGB1 and SARS-CoV-2-NP was performed using SARS-CoV-2 infected-mouse lung sections. The percentage of cytoplasmic HMGB1 (green) was determined. (E) The number of cytoplasmic HMGB1-positive cells was calculated using the ImageJ program. More than 100 cells per section were counted from each mouse section, and percentages are presented as means ± SD (n=4). (F, G) Lung sections from uninfected or SARS-CoV-2-infected mice were subjected to immunohistochemistry using anti-F4/80, anti-CD3ε, anti-CD45R, and anti-neutrophil Abs. The percentage of signal-positive cells was calculated using ImageJ program in the lung at 7 dpi. (H) The percentage of signal-positive cells was compared. More than 100 cells per section were counted from each mouse section. Data are expressed as means ± SD (n=4).
*p<0.01, **p<0.001, ***p<0.0001 vs. 0 dpi, *t*-test.

https://doi.org/10.4110/in.2023.23.e26

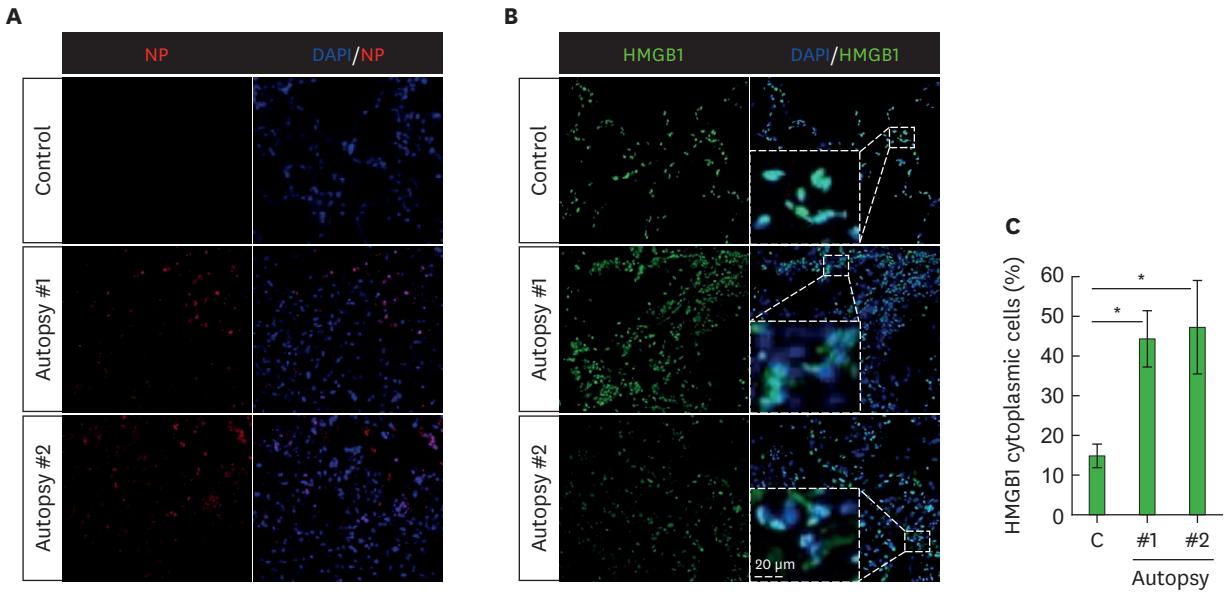

Figure 6. SARS-CoV-2-induced HMGB1 cytoplasmic translocation in human postmortem lungs. (A, B) Postmortem lung sections of a fatal SARS-CoV-2 case were stained with anti-SARS-CoV-2 NP (A) or anti-HMGB1 (B) Abs and with DAPI (blue). The percentage of cytoplasmic HMGB1 (green) was determined (C). The number of cytoplasmic HMGB1-positive cells over 100 cells per image (in total 4 images) was calculated using the ImageJ program. Data are presented as means ± SD.
*p<0.001 vs. control, one-way ANOVA with Tukey's multiple comparison test.

DISCUSSION

In this study, we demonstrated that active secretion and passive release of HMGB1 after SARS-CoV-2 infection are closely related to PTMs and PANoptosis. PTMs of HMGB1, including acetylation, phosphorylation, and oxidation, are involved in its active secretion via autophagosome formation and vesicular trafficking pathway (53). In our data, the levels of HMGB1 oxidation and phosphorylation in HEK293E/ACE2-C-GFP and Calu-3 cells could be observed with a peak at 6 hpi, leading to initiation of cytoplasmic translocation and secretion over 48 hpi *in vitro*. We detected markers of PANoptosis, including GSDMD cleavage, p-MLKL, and cleaved-caspase-3 after around 24 hpi of SARS-CoV-2. These cellular responses against SARS-CoV-2 were more sensitive in HEK293E/ACE2-C-GFP cells than in Calu-3 cells, probably due to ACE2 expression differences. SARS-CoV-2-related diseases are dynamic processes driven by the release of multiple cytokines and cell death, and a comprehensive understanding of the timeline of a late mediator of HMGB1 secretion under PTMs and PANoptosis can optimize treatment efficacy. In addition, a recent study showed that genetic depletion of HMGB1 protected SARS-CoV-2-infected cells from cell death, and HMGB1 inhibition reduced SARS-CoV-2 replication (54), suggesting that intracellular HMGB1 is a promising target molecule for the treatment of SARS-CoV-2 infection.

Pathogenesis of SARS-CoV-2 infection is a multi-organ dysfunction that triggers an uncontrolled immune response and is associated with sepsis and septic shock (55-58). HMGB1, one of the mediators of sepsis, can be released or secreted by pathogen infection and plays a pathological role in sterile inflammation or infection (27,41,42,59). The serum level of HMGB1 in the severe COVID-19 patients group was significantly higher than in the non-severe and normal groups (20). Also in our data, HMGB1 secretion levels were dramatically increased in HEK293E/ACE2-C-GFP and Calu-3 cells after SARS-CoV-2 infections. Therefore, the detection of elevated HMGB1 secretion levels can be used as a biomarker to determine infectious diseases such as SARS-CoV-2.

https://doi.org/10.4110/in.2023.23.e26

Excessive HMGB1 secretion is associated with various immune and pathogenic stresses. HMGB1 can bind to TLR2, TLR4, and TLR9 to induce inflammatory signaling and also to C1q to induce Ab-independent complement activation (60). HMGB1 could induce chemotaxis of neutrophils (61), which were observed here at 7 dpi in both mouse and human lung tissues. In this study, we observed that HMGB1 secretion level correlated with PTMs and PANoptosis. Our results strongly suggest that extracellular HMGB1 levels could be an indicator of the severity of SARS-CoV-2 infection. SARS-CoV-2 replication is generally decreased after 3–4 dpi in mouse study (62), however, HMGB1 level was still present at 7 dpi. Therefore, we are now investigating whether HMGB1 influences SARS-CoV-2 infection of neighboring cells and its replication.

ACKNOWLEDGEMENTS

This work was supported by grants from the National Research Foundation of Korea (NRF) funded by the Korean government (No. 2019R1A6A1A03032869 and 2022R1A2B5B03001446 to JSS, 2021R1I1A1A01044809 to MSK) and the Brain Korea 21 FOUR Project for Medical Science. DN Mai was supported by the MEF fellowship, which is part of the "Education and Research Capacity Building Project at the University of Medicine and Pharmacy at Ho Chi Minh City" implemented by the Korea International Cooperation Agency (KOICA) in 2023 (No. 2021-00020-2).

SUPPLEMENTARY MATERIALS

Supplementary Figure 1

ACE2 expression levels in HEK293E/ACE2-C-GFP and Calu-3 cells. WCLs of HEK293E/ACE2-C-GFP (HEK) and Calu-3 cells were collected, and subjected to western blot analysis using anti-ACE2 and β-actin Abs.

Click here to view

Supplementary Figure 2

SARS-CoV-2 infection induced HMGB1 release through PANoptosis. HEK293E/ACE2-C-GFP (A) and Calu-3 (B) cells were transfected with siRIPK3 and siCaspase-8 for 24 h, followed by infection with 0.1 MOI SARS-CoV-2 for 48 h. WCLs were subjected to SDS-PAGE and immunoblotted with anti-RIPK3, anti-caspase-8, and anti-β-actin Abs. Culture supernatants were harvested, and subjected to Western blot analysis using anti-HMGB1 and anti-β-actin Abs.

Click here to view

Supplementary Figure 3

Recombinant HMGB1 does not affect PANoptosis in HEK293E/ACE2-C-GFP and Calu-3 cells. HEK293E/ACE2-C-GFP (A) and Calu-3 (B) cells were treated with 5 μg/ml HMGB1 for the indicated times. WCLs were subjected to SDS-PAGE and immunoblotted with anti-GSDMD, anti-p-MLKL, anti-MLKL, anti-caspase-3, and anti-β-actin Abs.

Click here to view

REFERENCES

1. Kahn JS, McIntosh K. History and recent advances in coronavirus discovery. *Pediatr Infect Dis J* 2005;24:S223-S227.
PUBMED | CROSSREF
2. Cameroni E, Bowen JE, Rosen LE, Saliba C, Zepeda SK, Culap K, Pinto D, VanBlargan LA, De Marco A, di Iulio J, et al. Broadly neutralizing antibodies overcome SARS-CoV-2 omicron antigenic shift. *Nature* 2022;602:664-670.
PUBMED | CROSSREF
3. Choi JY, Smith DM. SARS-CoV-2 variants of concern. *Yonsei Med J* 2021;62:961-968.
PUBMED | CROSSREF
4. Shin DH, Smith DM, Choi JY. SARS-CoV-2 omicron variant of concern: everything you wanted to know about omicron but were afraid to ask. *Yonsei Med J* 2022;63:977-983.
PUBMED | CROSSREF
5. Yan R, Zhang Y, Li Y, Xia L, Guo Y, Zhou Q. Structural basis for the recognition of SARS-CoV-2 by full-length human ACE2. *Science* 2020;367:1444-1448.
PUBMED | CROSSREF
6. Lu R, Zhao X, Li J, Niu P, Yang B, Wu H, Wang W, Song H, Huang B, Zhu N, et al. Genomic characterisation and epidemiology of 2019 novel coronavirus: implications for virus origins and receptor binding. *Lancet* 2020;395:565-574.
PUBMED | CROSSREF
7. Kim S, Nguyen TT, Taitt AS, Jhun H, Park HY, Kim SH, Kim YG, Song EY, Lee Y, Yum H, et al. SARS-CoV-2 omicron mutation is faster than the chase: multiple mutations on spike/ACE2 interaction residues. *Immune Netw* 2021;21:e38.
PUBMED | CROSSREF
8. Hoffmann M, Kleine-Weber H, Schroeder S, Krüger N, Herrler T, Erichsen S, Schiergens TS, Herrler G, Wu NH, Nitsche A, et al. SARS-CoV-2 cell entry depends on ACE2 and TMPRSS2 and is blocked by a clinically proven protease inhibitor. *Cell* 2020;181:271-280.e8.
PUBMED | CROSSREF
9. Bayati A, Kumar R, Francis V, McPherson PS. SARS-CoV-2 infects cells after viral entry via clathrin-mediated endocytosis. *J Biol Chem* 2021;296:100306.
PUBMED | CROSSREF
10. Kang YW, Park S, Lee KJ, Moon D, Kim YM, Lee SW. Understanding the host innate immune responses against SARS-CoV-2 infection and COVID-19 pathogenesis. *Immune Netw* 2021;21:e1.
PUBMED | CROSSREF
11. Ren Y, Shu T, Wu D, Mu J, Wang C, Huang M, Han Y, Zhang XY, Zhou W, Qiu Y, et al. The ORF3a protein of SARS-CoV-2 induces apoptosis in cells. *Cell Mol Immunol* 2020;17:881-883.
PUBMED | CROSSREF
12. Li S, Zhang Y, Guan Z, Li H, Ye M, Chen X, Shen J, Zhou Y, Shi ZL, Zhou P, et al. SARS-CoV-2 triggers inflammatory responses and cell death through caspase-8 activation. *Signal Transduct Target Ther* 2020;5:235.
PUBMED | CROSSREF
13. Karki R, Sharma BR, Tuladhar S, Williams EP, Zalduondo L, Samir P, Zheng M, Sundaram B, Banoth B, Malireddi RK, et al. Synergism of TNF-α and IFN-γ triggers inflammatory cell death, tissue damage, and mortality in SARS-CoV-2 infection and cytokine shock syndromes. *Cell* 2021;184:149-168.e17.
PUBMED | CROSSREF
14. Ivanisenko NV, Seyrek K, Kolchanov NA, Ivanisenko VA, Lavrik IN. The role of death domain proteins in host response upon SARS-CoV-2 infection: modulation of programmed cell death and translational applications. *Cell Death Dis* 2020;6:101.
PUBMED | CROSSREF
15. Kuriakose T, Man SM, Malireddi RK, Karki R, Kesavardhana S, Place DE, Neale G, Vogel P, Kanneganti TD. ZBP1/DAI is an innate sensor of influenza virus triggering the NLRP3 inflammasome and programmed cell death pathways. *Sci Immunol* 2016;1:aag2045.
PUBMED | CROSSREF
16. Lee S, Karki R, Wang Y, Nguyen LN, Kalathur RC, Kanneganti TD. AIM2 forms a complex with pyrin and ZBP1 to drive PANoptosis and host defence. *Nature* 2021;597:415-419.
PUBMED | CROSSREF
17. Karki R, Lee S, Mall R, Pandian N, Wang Y, Sharma BR, Malireddi RS, Yang D, Trifkovic S, Steele JA, et al. ZBP1-dependent inflammatory cell death, PANoptosis, and cytokine storm disrupt IFN therapeutic efficacy during coronavirus infection. *Sci Immunol* 2022;7:eabo6294.
PUBMED | CROSSREF

18. Del Valle DM, Kim-Schulze S, Huang HH, Beckmann ND, Nirenberg S, Wang B, Lavin Y, Swartz TH, Madduri D, Stock A, et al. An inflammatory cytokine signature predicts COVID-19 severity and survival. *Nat Med* 2020;26:1636-1643.
PUBMED | CROSSREF

19. Karki R, Lee S, Mall R, Pandian N, Wang Y, Sharma BR, Malireddi RS, Yang D, Trifkovic S, Steele JA, et al. ZBP1-dependent inflammatory cell death, PANoptosis, and cytokine storm disrupt IFN therapeutic efficacy during coronavirus infection. *Sci Immunol* 2022;7:eabo6294.
PUBMED | CROSSREF

20. Wang H, Yang H, Czura CJ, Sama AE, Tracey KJ. HMGB1 as a late mediator of lethal systemic inflammation. *Am J Respir Crit Care Med* 2001;164:1768-1773.
PUBMED | CROSSREF

21. Chen R, Huang Y, Quan J, Liu J, Wang H, Billiar TR, Lotze MT, Zeh HJ, Kang R, Tang D. HMGB1 as a potential biomarker and therapeutic target for severe COVID-19. *Heliyon (Lond)* 2020;6:e05672.
PUBMED | CROSSREF

22. Bustin M, Reeves R. High-mobility-group chromosomal proteins: architectural components that facilitate chromatin function. *Prog Nucleic Acid Res Mol Biol* 1996;54:35-100.
PUBMED | CROSSREF

23. Bianchi ME, Beltrame M, Paonessa G. Specific recognition of cruciform DNA by nuclear protein HMG1. *Science* 1989;243:1056-1059.
PUBMED | CROSSREF

24. Lotze MT, Tracey KJ. High-mobility group box 1 protein (HMGB1): nuclear weapon in the immune arsenal. *Nat Rev Immunol* 2005;5:331-342.
PUBMED | CROSSREF

25. Watanabe T, Kubota S, Nagaya M, Ozaki S, Nagafuchi H, Akashi K, Taira Y, Tsukikawa S, Oowada S, Nakano S. The role of HMGB-1 on the development of necrosis during hepatic ischemia and hepatic ischemia/reperfusion injury in mice. *J Surg Res* 2005;124:59-66.
PUBMED | CROSSREF

26. Yanai H, Ban T, Wang Z, Choi MK, Kawamura T, Negishi H, Nakasato M, Lu Y, Hangai S, Koshiba R, et al. HMGB proteins function as universal sentinels for nucleic-acid-mediated innate immune responses. *Nature* 2009;462:99-103.
PUBMED | CROSSREF

27. Scaffidi P, Misteli T, Bianchi ME. Release of chromatin protein HMGB1 by necrotic cells triggers inflammation. *Nature* 2002;418:191-195.
PUBMED | CROSSREF

28. Kwak MS, Kim HS, Lee B, Kim YH, Son M, Shin JS. Immunological significance of HMGB1 post-translational modification and redox biology. *Front Immunol* 2020;11:1189.
PUBMED | CROSSREF

29. Bonaldi T, Talamo F, Scaffidi P, Ferrera D, Porto A, Bachi A, Rubartelli A, Agresti A, Bianchi ME. Monocytic cells hyperacetylate chromatin protein HMGB1 to redirect it towards secretion. *EMBO J* 2003;22:5551-5560.
PUBMED | CROSSREF

30. Youn JH, Shin JS. Nucleocytoplasmic shuttling of HMGB1 is regulated by phosphorylation that redirects it toward secretion. *J Immunol* 2006;177:7889-7897.
PUBMED | CROSSREF

31. Kim YH, Kwak MS, Park JB, Lee SA, Choi JE, Cho HS, Shin JS. *N*-linked glycosylation plays a crucial role in the secretion of HMGB1. *J Cell Sci* 2016;129:29-38.
PUBMED | CROSSREF

32. Ito I, Fukazawa J, Yoshida M. Post-translational methylation of high mobility group box 1 (HMGB1) causes its cytoplasmic localization in neutrophils. *J Biol Chem* 2007;282:16336-16344.
PUBMED | CROSSREF

33. Kwak MS, Kim HS, Lkhamsuren K, Kim YH, Han MG, Shin JM, Park IH, Rhee WJ, Lee SK, Rhee SG, et al. Peroxiredoxin-mediated disulfide bond formation is required for nucleocytoplasmic translocation and secretion of HMGB1 in response to inflammatory stimuli. *Redox Biol* 2019;24:101203.
PUBMED | CROSSREF

34. Davis K, Banerjee S, Friggeri A, Bell C, Abraham E, Zerfaoui M. Poly(ADP-ribosyl)ation of high mobility group box 1 (HMGB1) protein enhances inhibition of efferocytosis. *Mol Med* 2012;18:359-369.
PUBMED | CROSSREF

35. Schiraldi M, Raucci A, Muñoz LM, Livoti E, Celona B, Venereau E, Apuzzo T, De Marchis F, Pedotti M, Bachi A, et al. HMGB1 promotes recruitment of inflammatory cells to damaged tissues by forming a complex with CXCL12 and signaling via CXCR4. *J Exp Med* 2012;209:551-563.
PUBMED | CROSSREF

36. Yang H, Hreggvidsdottir HS, Palmblad K, Wang H, Ochani M, Li J, Lu B, Chavan S, Rosas-Ballina M, Al-Abed Y, et al. A critical cysteine is required for HMGB1 binding to Toll-like receptor 4 and activation of macrophage cytokine release. *Proc Natl Acad Sci U S A* 2010;107:11942-11947.
PUBMED | CROSSREF

37. Kazama H, Ricci JE, Herndon JM, Hoppe G, Green DR, Ferguson TA. Induction of immunological tolerance by apoptotic cells requires caspase-dependent oxidation of high-mobility group box-1 protein. *Immunity* 2008;29:21-32.
PUBMED | CROSSREF

38. Lu B, Nakamura T, Inouye K, Li J, Tang Y, Lundbäck P, Valdes-Ferrer SI, Olofsson PS, Kalb T, Roth J, et al. Novel role of PKR in inflammasome activation and HMGB1 release. *Nature* 2012;488:670-674.
PUBMED | CROSSREF

39. Qin S, Wang H, Yuan R, Li H, Ochani M, Ochani K, Rosas-Ballina M, Czura CJ, Huston JM, Miller E, et al. Role of HMGB1 in apoptosis-mediated sepsis lethality. *J Exp Med* 2006;203:1637-1642.
PUBMED | CROSSREF

40. Quarato G, Guy CS, Grace CR, Llambi F, Nourse A, Rodriguez DA, Wakefield R, Frase S, Moldoveanu T, Green DR. Sequential engagement of distinct MLKL phosphatidylinositol-binding sites executes necroptosis. *Mol Cell* 2016;61:589-601.
PUBMED | CROSSREF

41. Youn JH, Oh YJ, Kim ES, Choi JE, Shin JS. High mobility group box 1 protein binding to lipopolysaccharide facilitates transfer of lipopolysaccharide to CD14 and enhances lipopolysaccharide-mediated TNF-α production in human monocytes. *J Immunol* 2008;180:5067-5074.
PUBMED | CROSSREF

42. Youn JH, Kwak MS, Wu J, Kim ES, Ji Y, Min HJ, Yoo JH, Choi JE, Cho HS, Shin JS. Identification of lipopolysaccharide-binding peptide regions within HMGB1 and their effects on subclinical endotoxemia in a mouse model. *Eur J Immunol* 2011;41:2753-2762.
PUBMED | CROSSREF

43. Kwak MS, Lim M, Lee YJ, Lee HS, Kim YH, Youn JH, Choi JE, Shin JS. HMGB1 binds to lipoteichoic acid and enhances TNF-α and IL-6 production through HMGB1-mediated transfer of lipoteichoic acid to CD14 and TLR2. *J Innate Immun* 2015;7:405-416.
PUBMED | CROSSREF

44. Ivanov S, Dragoi AM, Wang X, Dallacosta C, Louten J, Musco G, Sitia G, Yap GS, Wan Y, Biron CA, et al. A novel role for HMGB1 in TLR9-mediated inflammatory responses to CpG-DNA. *Blood* 2007;110:1970-1981.
PUBMED | CROSSREF

45. Andersson U, Tracey KJ. HMGB1 is a therapeutic target for sterile inflammation and infection. *Annu Rev Immunol* 2011;29:139-162.
PUBMED | CROSSREF

46. Andersson U, Yang H, Harris H. Extracellular HMGB1 as a therapeutic target in inflammatory diseases. *Expert Opin Ther Targets* 2018;22:263-277.
PUBMED | CROSSREF

47. Xue J, Suarez JS, Minaai M, Li S, Gaudino G, Pass HI, Carbone M, Yang H. HMGB1 as a therapeutic target in disease. *J Cell Physiol* 2021;236:3406-3419.
PUBMED | CROSSREF

48. Chen J, Wang S, Blokhuis B, Ruijtenbeek R, Garssen J, Redegeld F. Cell death triggers induce MLKL cleavage in multiple myeloma cells, which may promote cell death. *Front Oncol* 2022;12:907036.
PUBMED | CROSSREF

49. Kim YH, Kwak MS, Lee B, Shin JM, Aum S, Park IH, Lee MG, Shin JS. Secretory autophagy machinery and vesicular trafficking are involved in HMGB1 secretion. *Autophagy* 2021;17:2345-2362.
PUBMED | CROSSREF

50. Kim DM, Kim Y, Seo JW, Lee J, Park U, Ha NY, Koh J, Park H, Lee JW, Ro HJ, et al. Enhanced eosinophil-mediated inflammation associated with antibody and complement-dependent pneumonic insults in critical COVID-19. *Cell Reports* 2021;37:109798.
PUBMED | CROSSREF

51. Cao DW, Liu MM, Duan R, Tao YF, Zhou JS, Fang WR, Zhu JR, Niu L, Sun JG. The lncRNA Malat1 functions as a ceRNA to contribute to berberine-mediated inhibition of HMGB1 by sponging miR-181c-5p in poststroke inflammation. *Acta Pharmacol Sin* 2020;41:22-33.
PUBMED | CROSSREF

52. Qu Y, Zhan Y, Yang S, Ren S, Qiu X, Rehamn ZU, Tan L, Sun Y, Meng C, Song C, et al. Newcastle disease virus infection triggers HMGB1 release to promote the inflammatory response. *Virology* 2018;525:19-31.
PUBMED | CROSSREF

53. Lee SA, Kwak MS, Kim S, Shin JS. The role of high mobility group box 1 in innate immunity. *Yonsei Med J* 2014;55:1165-1176.
PUBMED | CROSSREF

54. Kwak MS, Rhee WJ, Lee YJ, Kim HS, Kim YH, Kwon MK, Shin JS. Reactive oxygen species induce Cys106-mediated anti-parallel HMGB1 dimerization that protects against DNA damage. *Redox Biol* 2021;40:101858.
PUBMED | CROSSREF

55. Wei J, Alfajaro MM, DeWeirdt PC, Hanna RE, Lu-Culligan WJ, Cai WL, Strine MS, Zhang SM, Graziano VR, Schmitz CO, et al. Genome-wide CRISPR screens reveal host factors critical for SARS-CoV-2 infection. *Cell* 2021;184:76-91.e13.
PUBMED | CROSSREF

56. Stasi A, Castellano G, Ranieri E, Infante B, Stallone G, Gesualdo L, Netti GS. SARS-CoV-2 and viral sepsis: immune dysfunction and implications in kidney failure. *J Clin Med* 2020;9:4057.
PUBMED | CROSSREF

57. Chen YM, Zheng Y, Yu Y, Wang Y, Huang Q, Qian F, Sun L, Song ZG, Chen Z, Feng J, et al. Blood molecular markers associated with COVID-19 immunopathology and multi-organ damage. *EMBO J* 2020;39:e105896.
PUBMED | CROSSREF

58. Wiersinga WJ, Rhodes A, Cheng AC, Peacock SJ, Prescott HC. Pathophysiology, transmission, diagnosis, and treatment of coronavirus disease 2019 (COVID-19): a review. *JAMA* 2020;324:782-793.
PUBMED | CROSSREF

59. Wu M, Zou ZY, Chen YH, Wang CL, Feng YW, Liu ZF. Severe COVID-19-associated sepsis is different from classical sepsis induced by pulmonary infection with carbapenem-resistant klebsiella pneumonia (CrKP). *Chin J Traumatol* 2022;25:17-24.
PUBMED | CROSSREF

60. Wang H, Bloom O, Zhang M, Vishnubhakat JM, Ombrellino M, Che J, Frazier A, Yang H, Ivanova S, Borovikova L, et al. HMG-1 as a late mediator of endotoxin lethality in mice. *Science* 1999;285:248-251.
PUBMED | CROSSREF

61. Kim SY, Son M, Lee SE, Park IH, Kwak MS, Han M, Lee HS, Kim ES, Kim JY, Lee JE, et al. High-mobility group box 1-induced complement activation causes sterile inflammation. *Front Immunol* 2018;9:705.
PUBMED | CROSSREF

62. Berthelot F, Fattoum L, Casulli S, Gozlan J, Maréchal V, Elbim C. The effect of HMGB1, a damage-associated molecular pattern molecule, on polymorphonuclear neutrophil migration depends on its concentration. *J Innate Immun* 2012;4:41-58.
PUBMED | CROSSREF

63. Zheng J, Wong LR, Li K, Verma AK, Ortiz ME, Wohlford-Lenane C, Leidinger MR, Knudson CM, Meyerholz DK, McCray PB Jr, et al. COVID-19 treatments and pathogenesis including anosmia in K18-hACE2 mice. *Nature* 2021;589:603-607.
PUBMED | CROSSREF